Published in: *Journal of Geophysical Research*VOL.100-E10 21,119–21,234, October 25, 1995.

Low brightness temperatures of Martian Polar caps : CO_2 clouds or low surface emissivity ?

François Forget

Laboratoire de Météorologie Dynamique du CNRS, Ecole Normale Supérieure, Paris, France.

Gary B. Hansen

Geophysics Program, University of Washington, Seattle

James B. Pollack[1]

Space Science Division, NASA Ames Research Center, Moffett Field, California

Abstract. One of the major surprises from the spacecraft missions to Mars of the 1970s was the finding of anomalously low brightness temperatures in the winter polar regions, far below the CO_2 frost point expected for the Martian polar caps. The location and brightness temperatures of these areas sometimes varied on timescales of days. Many explanations have been advanced for this puzzling behavior, including the low emissivities of carbon dioxide frost and the presence of carbon dioxide clouds. In the past, several authors have argued in favor of or against both hypotheses, but no conclusion has been reached. We have carefully analyzed the thermal emission measurements obtained by the Mariner 9 infrared interferometer spectrometer (IRIS) and the Viking infrared thermal mapper (IRTM). Besides their low brightness temperatures, the anomalous areas are characterized by their complex spectral signature. Also, there is evidence suggesting that their occurrence is related to the condensation of CO_2 in the atmosphere. We have used a combination of data analysis and modeling to compare these observations with simulated spectra obtained with radiative models of CO_2 ice clouds and CO_2 ice deposits. Only precipitating CO_2 cloud with particle radius larger than 10 μm and CO_2 snow deposits with millimeter-sized grains are able to produce the observed features. In both cases, matching the IRIS spectra requires the CO_2 ice particles to be mixed with small amounts of water or dust, as expected for the northern winter cap observed by the Mariner 9 mission. Nonprecipitating CO_2 clouds, if they exist, should be transparent in the infrared. On the other hand, CO_2 ice deposits composed of large grains or monolithic ice which have directly condensed on the ground could have an emissivity close to unity and in any case much higher than that of small CO_2 ice particles originating from atmospheric condensation. We conclude that the low brightness temperatures are likely to be created by CO_2 snow falls and that both falling snow particles and fresh snow deposits could contribute to create the observed features.

1. Introduction

A unique and very important aspect of the current climate of Mars is the seasonal CO_2 cycle. During the fall and winter seasons, the local surface and atmospheric temperatures fall to the frost point of CO_2 gas, CO_2 condenses, and polar ice caps are formed. The surface temperature of the polar CO_2 ice deposits is thus controlled by vapor-pressure equilibrium. At the expected atmospheric pressure on the polar caps, about 6 millibars, this temperature should be about 148 K.

[1]Deceased, June 13, 1994.

A major surprise from the spacecraft missions of the 1970s was the finding of areas in the winter polar regions with anomalously low brightness temperatures at 20-μm wavelength, some below 135 K [*Kieffer et al.*, 1976b].

The location and brightness temperatures of these areas (hereafter also called "cold spots") sometimes varied on timescales of days [*Kieffer et al.*, 1977], suggesting complex physical processes. By altering the infrared emission toward space, these cold spots are likely to have a strong impact on the polar energy balance. In particular, the amount of CO_2 that condenses in the caps is controlled by the energy balance of the polar regions. To first approximation, during the polar night, the latent heat released by the condensation of CO_2 balances the net infrared radiation toward space. Therefore the cold spots could strongly decrease our estimates of the total amount of CO_2 that condenses during the winter and may themselves affect the global climate on Mars [*Kieffer et al.*, 1976b].

Hypotheses for explaining these anomalously low brightness temperatures include a strong enrichment in lighter, noncondensible gases in the winter polar atmosphere allowing the partial pressure of CO_2 to be less than that at low latitude [*Kieffer et al.*, 1977], low emissivities for carbon dioxide frost [*Ditteon and Kieffer*, 1979], and the presence of carbon dioxide clouds [*Hunt*, 1980]. *Hess* [1979] cast doubt on the feasibility of the noncondensible gas enrichment by showing that vertical and horizontal gradients in the average molecular weight of the Martian polar atmosphere could be stable only under very special circumstances. The last two hypotheses have been supported or studied by various authors. See *Ditteon and Kieffer* [1979], *Warren et al.* [1990], and *Hansen* [1994] for the low surface emissivity hypothesis, and *Hunt* [1980], *Paige* [1985], *Paige et al.* [1990], *Pollack et al.* [1990], and *Forget and Pollack* [1993] for the CO_2 clouds scenario. Until now, it has not been possible to conclusively solve the puzzle because of the complexity of the problem and the lack of data. Besides, the two hypotheses may not be contradictory since the spectral properties of thick CO_2 clouds and surface frost of similar effective grain size should be close.

What causes the anomalously low brightness temperatures? To address this important issue, we have tried to use all the thermal infrared data available to study the spectral, spatial, and temporal properties of the cold spots in order to learn more about the possible mechanisms involved and to assess the hypotheses.

Two complementary data sets are currently available: Mariner 9 infrared interferometer spectrometer (IRIS) spectra and Viking infrared thermal mapper (IRTM) brightness temperatures. The IRIS spectra provide a good definition of the spectral properties of the winter polar atmosphere and surface but only for a limited range of seasonal dates and locations and with poor spatial resolution. Conversely, the IRTM data provide good coverage of both polar regions over the relevant seasons but in only three spectral channels.

In sections 2 and 3, we present in more detail the characteristics of these data and the typical features observed in the cold spots. In sections 4 and 5, we analyze the CO_2 clouds and the low-emissivity scenarios and compare them to the observations. In section 6, we conclude by suggesting a new realistic scenario consistent with the observations, and discuss its implications.

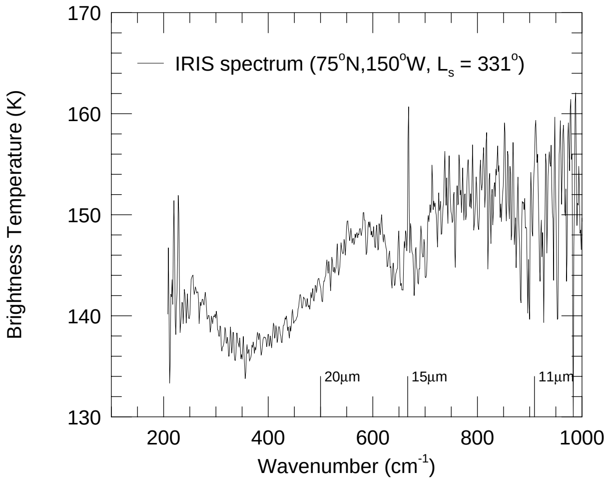

Figure 1. Typical northern winter polar Mariner 9 IRIS spectrum. This particular spectrum was obtained at 75^oN,150^oW and L_s = 331^o (Data Acquisition System time : 6320999, Orbit 132, emission angle : 59.5^o). Data below 225 cm^{-1} and above 750 cm^{-1} are very noisy and thus not reliable. Center wavenumbers of three of the IRTM channels are also indicated.

2. Mariner 9 IRIS Spectra

2.1. Data Set

The Mariner 9 IRIS was a Michelson interferometer with a spectral resolution of 2.4 cm^{-1} [*Hanel et al.*, 1972; *Conrath et al.*, 1973]. At low temperatures (T <150 K), data are reliable only in the range 11-45 μm. More than 20,000 spectra were obtained during the Mariner 9 mission of which 1800 were taken above the seasonal polar caps poleward of 50^o latitude. Unfortunately, almost all these spectra were obtained only in the northern hemisphere at the end of winter, between the areocentric longitude of the Sun (L_s, defined to be 0^o at the northern vernal equinox) of 322^o and 351^o. The field of view of the instrument was circular with a diameter of 4.5^o. As most polar IRIS spectra were obtained from an altitude of about 4000 km, this corresponds to a 315-km-diameter footprint for nadir viewing and to a 370-km by 580-km elliptical footprint for emission angles near 50^o, a typical value in the dataset.

The Mariner 9 spacecraft arrived at Mars during a major global dust storm, and the atmosphere was extremely dust-laden during much of the primary mission. However, *Hanel et al.* [1972] reported that the dust was dissipating by L_s=319^o, and clearing was well advanced by L_s=341^o.

2.2 Characteristic features

Most IRIS spectra obtained during the northern winter above the polar caps exhibit the same complex spectral signature. Many of them unambiguously present anomalously low brightness temperatures (Fig. 1).

The prominent feature extending from about 600 to 800 cm^{-1} is due to absorption and emission by gaseous CO_2. Centered at 667 cm^{-1} (15 μm) is the strongest absorption band, the vibrational bending fundamental of CO_2 (ν_2 of $^{12}C^{16}O_2$). On both sides of this 15-μm feature are a number of weaker combination, isotopic, and hot bands. The observed signature in Fig. 1 (the 667 cm^{-1} feature in emission and the weak bands in absorption) is representative of the IRIS spectra displaying low brightness temperatures. It suggests a strong inversion, high in the atmosphere, and below that, a much colder atmosphere within which temperature decreases with increasing altitude. This temperature structure is consistent with the Mariner 9 radio occultation profiles [*Kliore et al.*, 1972]. In some other polar IRIS spectra (not shown here), the temperature inversion seems to start at a lower altitude. The 15-μm band then corresponds to a single warm feature. However, these spectra do not usually display anomalously low brightness temperatures.

Outside the CO_2 band, minimum brightness temperatures generally occur around 350 cm^{-1}, and local maxima exist over a broad region around 850 cm^{-1} and a region near 250 cm^{-1}. Interpreting such a large emission and absorption feature is not straightforward. This signature does not point clearly to a surface or an atmospheric component. We shall test different scenarios through their ability to reproduce these features, as well as the 15-μm profile.

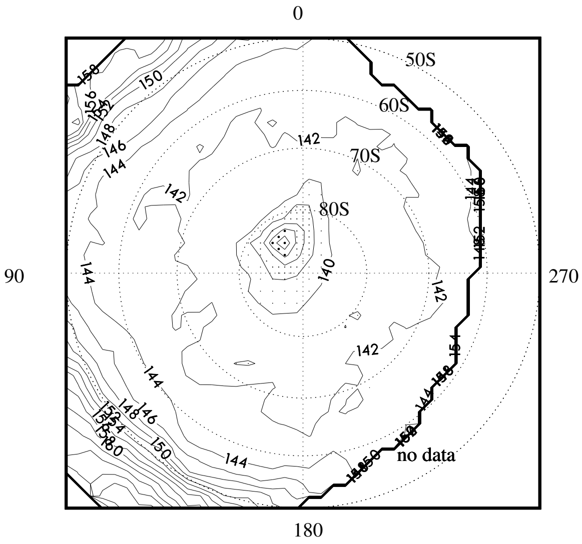

Figure 2. IRTM T_{20} measured by the Viking Orbiter 2, orbit 79, in the south polar region in winter ($L_s = 145.8^o$). The contour interval is 2 K. The minimum temperature in the cold spot near the pole is 129 K.

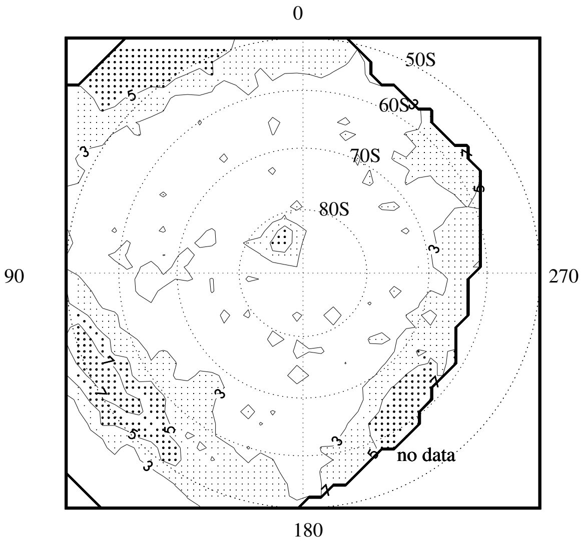

Figure 3. South polar region. Map of $T_{11} - T_{20}$ corresponding to Fig. 2 ($L_s = 145.8^o$). The contour interval is 2 K.

3. Viking Infrared Thermal Maps

3.1 Dataset

The two Viking orbiters observed the entire planet during almost two Martian years [see *Kieffer et al.*, 1977]. The infrared thermal mappers (IRTM) operated in five broad infrared channels, but only the 11-, 15-, and 20-μm channels are reliable for studying very cold areas like the Martian polar caps (the 7- and 9-μm channels are too noisy). The 11- and 20-μm channels are unaffected by gaseous absorption. They measure the surface brightness temperature when aerosol (dust, H_2O ice, or CO_2 ice) opacity is low at these wavelengths. When the aerosol opacity is large enough, the 11- and 20-μm brightness temperatures are influenced by the presence of the aerosols which can absorb, reemit, and scatter the ground emission. The 15-μm channel, with a spectral response centered on the strong gaseous CO_2 absorption feature, measures atmospheric temperatures over a broad altitude range with maximum sensitivity near the 0.6-mbar pressure level [*Kieffer et al.*, 1976a].

The field of view of each channel was defined by focal plane stops 5.2 mrad in diameter. The corresponding footprint diameter generally ranged from 5 to 30 km in the north polar region, and from 10 to 200 km in the south polar region.

3.2 Characteristic Features

Spatial characteristics. We have plotted and analyzed more than 100 maps from the IRTM data, and performed numerous diagnostics and data analyses. A complete description of the climatology of the winter polar caps during the Viking years is beyond the scope of the present paper and

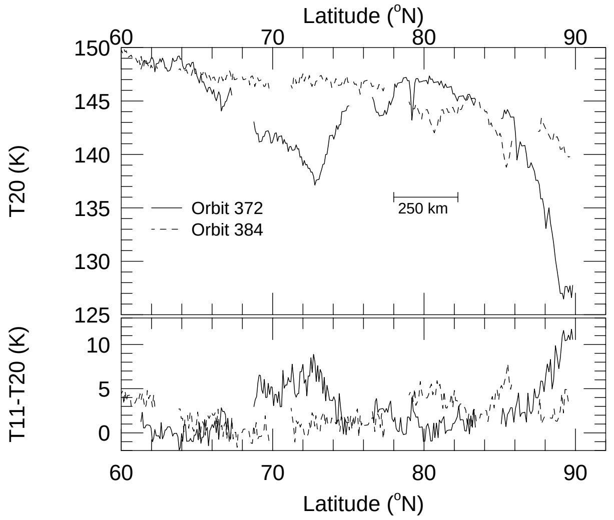

Figure 4. The brightness temperature T_{20} and the $T_{11} - T_{20}$ spectral difference observed in two similar south-north scans taken by Viking Orbiter 2 (IRTM detector 7) on orbits 372 (L_s = 322.9^o) and orbit 384 (L_s = 329.2^o) along meridian 183^{o}W.

will be the subject of a future publication. We shall focus here on the characteristic features likely to be of interest for our investigation.

The difference $T_{11} - T_{20}$ (also called "spectral contrast") is a useful tool for characterizing the radiative properties of the atmosphere and the surface. (The spectral contrast of a blackbody would be zero.) Fig. 2 and 3 show typical thermal maps of the fall or winter southern cap. Generally, and for these maps in particular, characteristic features are observed: Around the cap, there are large areas of positive values of $T_{11} - T_{20}$ (typically 3 to 5 K, up to 7 to 10 K on the dayside). Inside the cap, $T_{11} - T_{20}$ values are positive but remain close to 0 K. Near the pole, high values of $T_{11} - T_{20}$ (up to 12 K) are observed where cold spots (low values of T_{20}) are present.

In the northern hemisphere, the same type of features are observed except that cold spots were more common at lower latitudes down to 60^{o}N. Most of the time, the observed $T_{11} - T_{20}$ background values inside the cap were higher than in the south, reaching values up to 4 K as compared to 0 to 1 K in the south.

Fig. 4 shows the brightness temperatures measured during two similar low altitude scans by the Viking Orbiter 2 during orbits 372 and 384 in the middle of the northern winter. Both orbits scanned the same meridian at 183^{o}W from the midlatitudes to the pole. Despite the fact that these observations were only 12 Martian days apart and that they correspond to exactly the same areas, they exhibit very different brightness temperature structures. This illustrates the high variability of the anomalously low brightness temperatures. However, we have found in other observations that many characteristic small structures similar to the dip observed during orbit 372 at 79^{o}N fluctuate but in most cases do not move. In many cases these fluctuating cold spots appear to be well correlated with the locations of surface features such as the permanent polar cap boundaries or isolated craters, suggesting that topography could play a role in the origin of the cold spots. Both scans were taken one measurement every 6 km (except for a few large gaps), with a spatial resolution ranging from 5 km at 60^{o}N up to 11 km near the pole. This good spatial sampling reveals fine structures with spatial scales as low as a few tens of kilometers. The variations of $T_{11} - T_{20}$ are also shown in Fig. 4. Here again, despite the fact that T_{11} is noisy, these variations are clearly related to the variations of T_{20}.

Seasonal evolution. The temporal evolution of T_{11} and T_{20} on both polar caps is illustrated in Fig. 5 where we have plotted averaged values of T_{11} and T_{20} for different latitude belts, binned every 5 solar longitude deg. (See also the frames published by *Martin* [1981].) The variation of these averaged values reflects the variation of the frequency and intensity of the cold spots, except in the northern hemisphere where T_{11} and T_{20} were also affected by atmospheric dust during the second Viking global dust storm just after the winter solstice.

No particular features appear on the southern hemisphere plots, where the cold spot distribution seemed to be rather constant, except at the pole where the mean T_{20} reached a minimum in early winter (L_s=110^o-120^o). In the northern hemisphere, the second dust storm of the first "Viking year" started at L_s=273^o. As mentioned above, the presence of dust above the polar caps is detected by a strong warming of T_{20} and T_{11} between L_s=275^o and L_s=290^o, especially at lower latitudes. Poleward of 70^o north, the dust storm was followed by a period of minimum mean brightness temperatures. A careful study of the data shows that an exceptionally high frequency of occurrence of extremely low brightness temperatures was reached near the pole around L_s=300^o, right after the first phase of the storm. This apparent correlation between airborne dust and cold spots is a very important and striking characteristic of the IRTM data.

Correlation between T_{11} and T_{20}. As suggested by the $T_{11} - T_{20}$ and T_{20} maps and scans, the cold spots are characterized by large values of $T_{11} - T_{20}$ [*Paige*, 1985]. Fig. 6 shows the correlation of T_{20} and $T_{11} - T_{20}$ for the northern and southern hemispheres. The observed linear correlation is almost always observed during the winter and fall seasons. Such behavior is also a key characteristic of the cold spots. The difference between the two hemispheres is likely to be due to a difference in surface temperature, the south pole being colder than the north pole [*Paige and Ingersoll*, 1985].

Interpreting differences between T_{11} and T_{20} is not straightforward. Several different processes can produce such a signature.

First, one must keep in mind that the noise level of the 11-μm channel has to be considered (it can be neglected for the 20-μm channel). The temperature equivalent noise of T_{11} is about 1.6 K at 150 K , 2.6 K at 140 K, 3.4 K at 135 K and

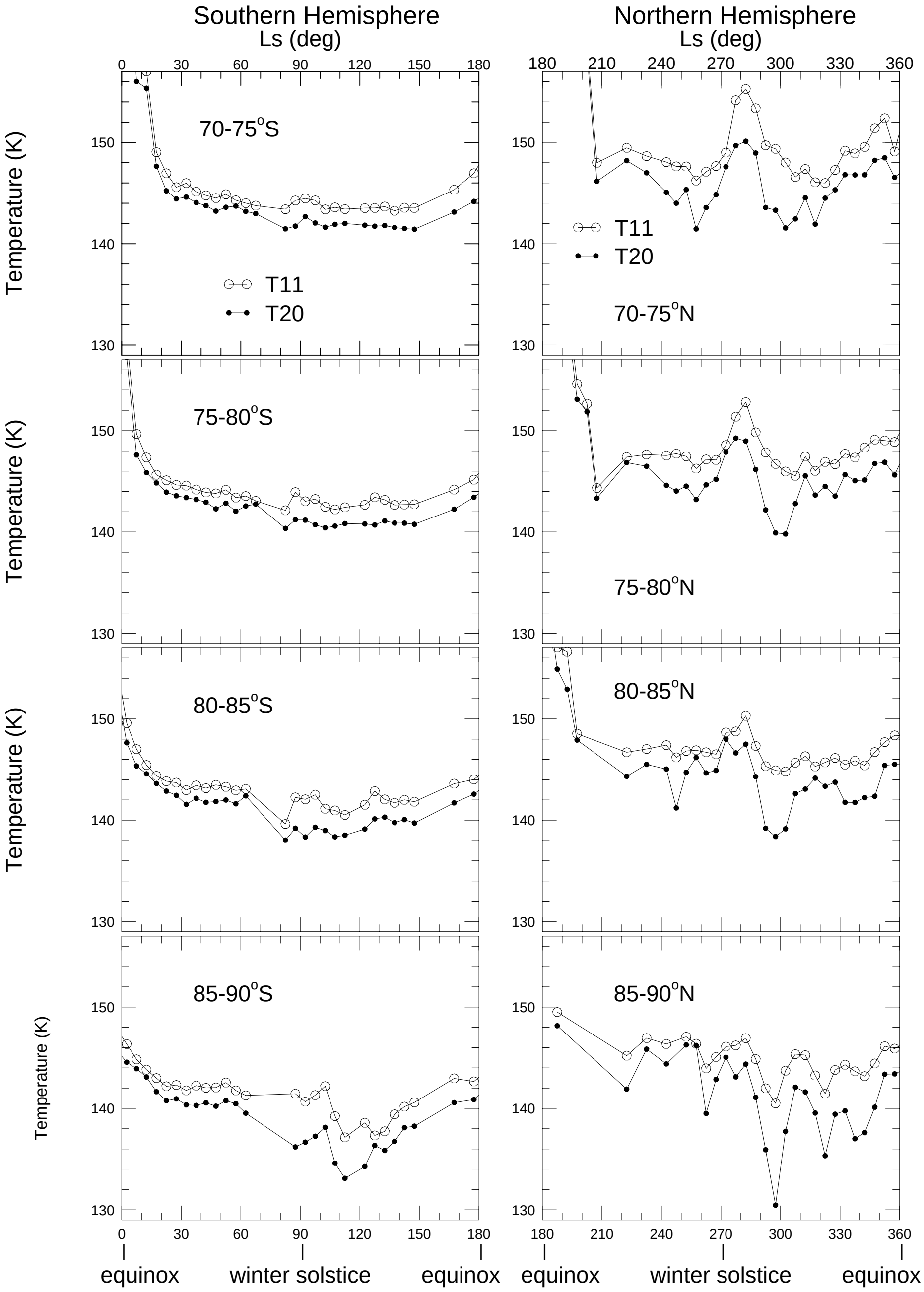

Figure 5. Seasonal evolution of IRTM brightness temperatures, averaged in 5^o lat by 5^o L_s bins.

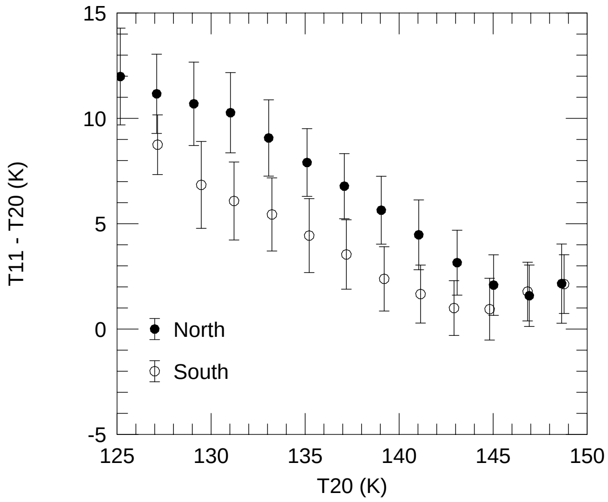

Figure 6. Correlation between T_{20} and $T_{11} - T_{20}$ in both hemispheres, poleward of 70^o, with emission angles below 60^o. Data are averaged in 2 K bins. The variability in the data is illustrated by the error bars showing the standard deviation ($\pm\sigma$).

4.6 K at 130 K. As this noise is random, it cannot explain the systematic bias observed at the cold spots.

Physically, $T_{11} - T_{20}$ differences can be produced by (1) nonunit thermal emissivity of the ground (either because it is a non gray emmissivity or a gray emissivity which is less than unity), (2) the presence of atmospheric aerosols (dust or ice clouds), or (3) nonuniform temperature across the field of view of the instrument. For example, the high values of $T_{11} - T_{20}$ observed at the polar cap boundary in Fig. 3 must be due to a combination of water ice clouds (known to be present especially near the polar cap edge) and non uniform temperatures (viewing a scene whose area includes both relatively warm bare ground and cold patches of ice produces substantial spectral differences) [*Christensen and Zurek*, 1984]. In the cold spots, dust could theoretically play a role in the infrared emission. In fact, the dust extinction coefficients in the 11- and 20-μm bands are not very different. Thus the dust is not expected to have a strong impact on $T_{11} - T_{20}$ above the polar cap, at least during the "clear" period, outside the dust storms. Non uniform temperatures could theoretically be observed when CO_2 ice on the ground (at 150 K) shares the IRTM field of view with a colder object such as a CO_2 or H_2O cloud higher in the atmosphere. However, the maximum value of $T_{11} - T_{20}$ obtained in such a case (with 60% at 130 K, and 40% at 150 K) would only reach 1.4 K, whereas actual spectral differences are about 8 to 10 K. To summarize, let's repeat that not only are the low brightness temperature areas characterized by low values of T_{20} but also by large and systematic differences between T_{11} and T_{20}, and that such a spectral contrast can similarly be attributed to the presence of CO_2 or H_2O clouds, or nonunit thermal emissivity of the ground.

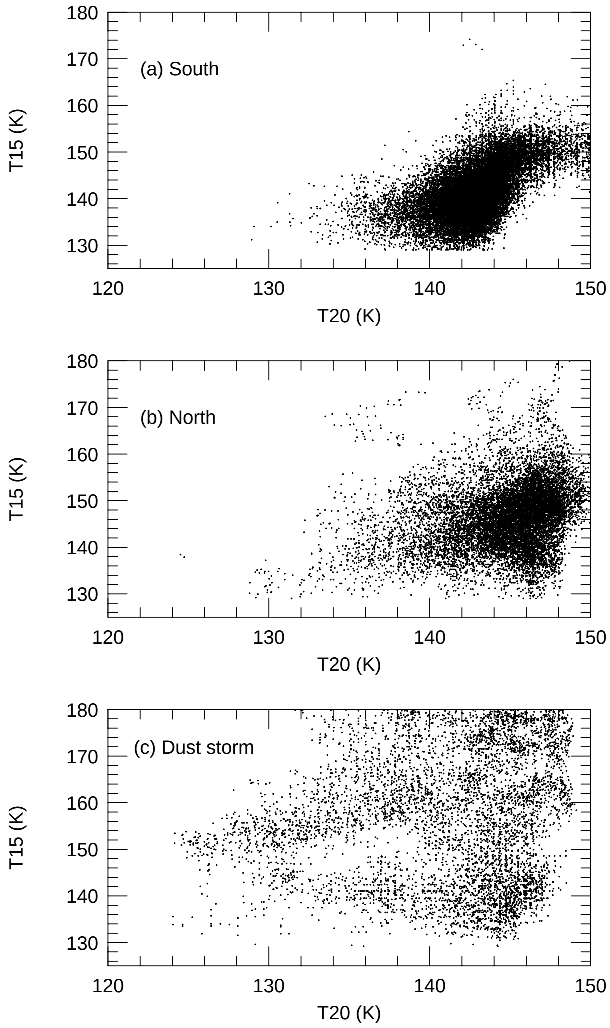

Figure 7. Correlation between T_{15} and T_{20} (Included are the observations poleward of 70^o lat, with an emission angle below 45^o) : *a*) in the southern hemisphere ($0^o > L_s > 180^o$) *b*) in the northern hemisphere outside dust storm b ($180^o > L_s > 270^o$ and $320^o > L_s > 360^o$) *c*) in the northern hemisphere during dust storm b and the polar warming event ($270^o > L_s > 320^o$)

Correlation between T_{15} and T_{20}. Fig. 7a. shows the observed correlation between T_{20} and the atmospheric brightness temperatures T_{15} in the southern hemisphere. We included all the IRTM observations obtained poleward of 70°S during the fall and winter seasons, with an emission angle lower than 45° (about 25,000 data points). T_{15} is never below 129.5 K, which corresponds to the emission of an atmosphere following the coldest possible temperature profile at every altitude: the CO_2 frost point temperature profile. A very interesting feature is the tendency for T_{15} to decrease toward this minimum value with decreasing values of T_{20}. This means that cold spots could be related in some way to cold atmospheric temperatures. The same type of plot for the northern hemisphere data obtained during the fall and winter seasons outside the period of the second Viking dust storm is shown in Fig. 7b. A similar kind of correlation is observed, especially for the low T_{20} values. The unusual cluster of points with $T_{15} > 160\ K$ and $T_{20} < 140\ K$ corresponds to a single set of observations obtained around 71°N-0°W during VO2 orbit 242 at L_s=247.9°N.

During the second Viking dust storm, the Martian polar atmosphere experienced a rapid and intense warming event observed by the IRTM instrument, caused by complex atmospheric dynamical processes [*Martin and Kieffer*, 1979; *Jakosky and Martin*, 1987]. Fig. 7c shows that these high values of T_{15} were also observed in the anomalously cold temperature areas, which were, as mentioned above, particularly common then.

4. CO_2 Clouds Hypothesis

4.1 Existence of CO_2 Clouds

As first suggested by *Gierasch and Goody* [1968], further studied by *Paige* [1985] using a one-dimensional polar radiative model, and more recently modeled and analyzed with a general circulation model [*Pollack et al.*, 1990], atmospheric CO_2 condensation could occur at most altitudes of high latitudes during the fall and winter seasons. CO_2 ice particles are likely to form clouds in the polar night atmosphere (see review in work by *James et al.* [1992]).

Definitive observational evidence does not exist. Clouds in the polar regions of Mars during the fall and winter seasons have been known to astronomers for decades, especially in the northern hemisphere and are referred to as "polar hoods" [see *Briggs and Leovy*, 1974; *Briggs et al.*, 1977] However, Mariner 9 IRIS showed that the northern winter hood was composed of water ice, at least south of 65°N. *Briggs and Leovy* [1974] observed at higher latitudes some cloud lines formed at the CO_2 ice temperature, with very distinct small structure. They showed that water ice clouds could not have exhibited such a structure because of the slow condensation and sublimation rates of water ice at low temperature and that these clouds were likely to be composed of CO_2 ice. Also, three of the Mariner 6 and 7 infrared spectrometers limb spectra have been interpreted as a reflection on thin CO_2 clouds because of characteristic spikes at 4.26 μm [*Herr and Pimentel*, 1970].

4.2 Link Between Low Brightness Temperatures and Atmospheric CO_2 Condensation

Kieffer et al. [1976b] first suggested that CO_2 clouds could create the anomalously low IRTM brightness temperatures, among other possibilities. *Pollack et al.* [1990] showed that the spatial and temporal variabilities of the modeled atmospheric condensation rate were consistent with those exhibited by the low 20-μm brightness temperatures mapped by the Viking IRTM [*Kieffer et al.*, 1977]. We have seen above that the IRTM measurements in the 15-μm gaseous CO_2 band shown in Fig. 7 also suggested a link between the cold spots and low atmospheric temperatures, at least outside the dust storm periods and the related polar warming events. Above all, the fact that the second Viking dust storm was followed by a period of maximum frequency and intensity of low brightness temperature events strongly supports the notion that the low brightness temperatures are due to the condensation of CO_2 ice in the atmosphere. Several studies have shown the link between dust and CO_2 atmospheric condensation [*Paige*, 1985; *Pollack et al.*, 1990]. The dusty atmosphere experiences much greater cooling than a clear atmosphere because of the significant infrared emissivity of the dust particles. This results in an enhanced atmospheric condensation rate. Model calculations indicate that increasing the dust optical depth from 0 to 5 in the winter polar atmosphere produces a transition from a situation in which almost all the carbon dioxide condenses on the ground to one in which it nearly all condenses in the atmosphere. It also seems likely that the dust particles can serve as condensation nuclei.

4.3 Radiative Properties of CO_2 Clouds

How can CO_2 clouds lower the brightness temperature emitted to space? In fact, the radiative properties of CO_2 clouds are poorly known. *Ditteon and Kieffer* [1979] first measured that the interband absorption coefficients of CO_2 ice in the thermal infrared were very small. Recent laboratory measurements by G. B. Hansen (Spectral coefficient of CO_2 ice, 2. Thermal Infrared, manuscript in preparation for *JGR-Planets*, 1995) indicate that in the spectral regions on either side of the strong 15-μm absorption, the CO_2 ice is actually a factor of 10 more transparent than reported by Ditteon and Kieffer.

Therefore pure CO_2 ice clouds should not absorb and emit much radiation themselves. On the basis of the laboratory data of Ditteon and Kieffer, *Hunt* [1980] showed that CO_2 clouds could lower the brightness temperatures emitted to space by scattering the radiation emitted by the surface back to the surface which would ultimately absorb the redirected photons. *Hunt* [1980] computed that a cloud of only modest optical thickness composed of particles of 10-μm radius over a ground with effective temperature of 150 K could produce brightness temperatures of about 130 K.

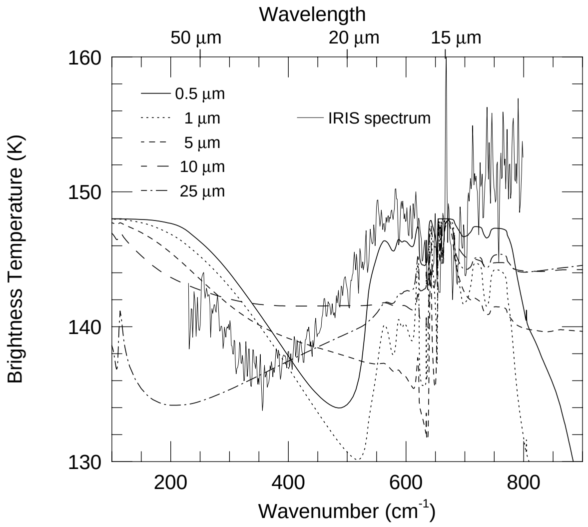

Figure 8. Same spectrum as in Fig. 1, compared to simulated spectra of pure CO_2 clouds with various particle radii and a similar emission angle (60^o). The clouds all have a vertical optical thickness of of $\tau = 1$ at 500 cm^{-1} (20-μm). The temperatures of cloud and ground are 148 K.

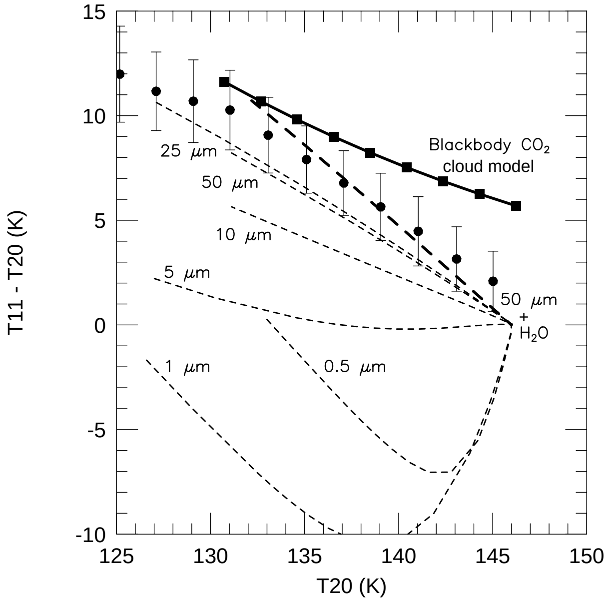

Figure 9. Dashed lines : Correlation between T_{20} and T_{11} simulated with pure CO_2 clouds for various cloud particle radii compared to the observed brightness temperatures. The line of long thick dashes is the simulated correlation for CO_2 cloud (particle radius $r = 50\mu$m) contaminated by 2 pr-μm of H_2O ice ($r = 1\mu$m) . Correlations were computed by varying the cloud optical depth at 20 μm from 0 to 4. The temperatures of cloud and ground are 146 K. The line with square symbols corresponds to the expected correlation for blackbody clouds at various temperatures lying below a "constant" H_2O cloud at 165 K. The northern hemisphere IRTM data shown for comparison are the same as in Fig. 6.

On the basis of the more reliable data from G. B. Hansen, we have simulated the signature of pure CO_2 ice clouds with a radiative transfer program that allows for absorption, scattering, and emission by atmospheric aerosols [*Toon et al.*, 1989; *Pollack et al.*, 1993]. This algorithm is based on the two-stream, hemispheric mean, source function solution to the equation of radiative transfer and allows for the emission angle of the observations. The single-scattering calculation follows Mie theory, and we assume that we can mimic the signature of a Martian CO_2 clouds by a model cloud of "equivalent spheres". We used a Hansen-Hovenier gamma particle size distribution with an effective variance of 0.05, equivalent to a lognormal distribution with $\sigma_g = 0.221$ [*Hansen and Travis*, 1974].

Fig. 8 shows the signature of CO_2 clouds with a vertical optical thickness at 20 μm of one and a viewing angle of 60^o for various particle sizes. We show in Table 1 the amount of CO_2 ice required to reach such an optical thickness.

4.4 Small-Particle CO_2 Clouds

Particles with a cross-section-weighted average radius smaller than 0.5 μm are too small to effectively scatter the infrared radiation below 1000 cm^{-1}. Since CO_2 ice cannot absorb outside the 15-μm band, huge quantities are required to obtain the observed optical depth around 300-500 cm^{-1} (Table 1). In fact, pure CO_2 ice clouds composed of small particles with a mode radius smaller than 1 μm are likely to be transparent in the thermal infrared.

Particles with a radius larger than 1 μm can more readily scatter the infrared radiation. Outside the 15-μm band and below 200 cm^{-1} they are almost conservative scatterers with a single-scattering albedo close to one for the studied spectral regions. Their signature is not dependent upon the cloud temperature. However, for particle radius between 1 and 5 μm , the ability to reduce the infrared fluxes toward space increase with wavenumber on the relevant spectral interval (below 1000 cm^{-1}). Such a signature is very different than what is observed in the IRIS spectra. Moreover, simulation of IRTM brightness temperatures then gives T_{11} lower than T_{20}, which is never observed in the IRTM data (Fig. 9).

CO_2 clouds could be composed of CO_2 ice contaminated by "impurities" such as water or dust. The presence of water ice clouds in the observed polar hood implies that water ice could also be present in the polar night areas and it seems likely that some dust is present in the winter polar regions as a result of transport from lower latitudes. Such contaminents could decrease the single scattering albedo of the cloud particles. CO_2 clouds composed of "contaminated" particles able to absorb and reemit the radiation could lower the brightness temperatures emitted to space not only because of their ability to backscatter the radiation, but because of their colder effective temperatures. (the frost point of CO_2 is 140 K at 1.8 mbar, 135 K at 0.8 mbar, 130 K at 0.4 mbar). Could the signature of such contaminated CO_2 clouds match the observations? In fact the CO_2 ice absorption coefficients

Particle radius μm	Q_{ext} (at 20-μm)	Mass for $\tau_{20\mu\mathrm{m}} = 1$ kg.m^{-2}	Sedimentation speed m.s^{-1}
0.1	1.1 10^{-5}	19.6	8.3 10^{-5}
0.5	1.7 10^{-4}	6.35	4.4 10^{-4}
1	2.5 10^{-3}	0.86	9.6 10^{-4}
5	0.763	1.4 10^{-2}	7.5 10^{-3}
10	2.95	7.3 10^{-3}	2.2 10^{-2}
25	2.50	2.2 10^{-2}	1.0 10^{-1}
50	2.35	4.6 10^{-2}	3.8 10^{-1}
100	2.19	9.9 10^{-2}	1.42

Table 1. The extinction parameter Q_{ext} at 20-μm and the corresponding mass of airborne CO_2 ice per square meter required to make a cloud with an optical thickness equal to one for various CO_2 ice cloud particle sizes. Last column shows the sedimention speed (in meters per second) of these particles on Mars at the 5-mb pressure level. The sedimentation speed was estimated using the Stokes formulae, modified for low pressure (Knudsen number below unity), following Rossow (1978).

measured in the weak bands show that pure CO_2 ice presents a "window" in absorption between 20 μm (500 cm^{-1}) and 40 μm (250 cm^{-1}). If the CO_2 cloud is not transparent, but not really opaque, its expected signature would be a region of higher temperature in this window compared to the band on each side (at least if the cloud extinction is dominated by absorption). This is exactly the opposite of what is observed in the IRIS spectra. Water ice contamination cannot change this behavior since water ice presents a similar window in absorption between two water ice absorption bands centered at 12.2 (820 cm^{-1}) and 45 μm (222 cm^{-1}).

4.5 Precipitating CO_2 Clouds

Particles with radius larger than 10 μm are not expected to stay airborne over long periods (Table 1). Above 25 μm they are likely to fall out the atmosphere rapidly. Unless unexpected vertical winds occur in the winter polar regions, CO_2 clouds composed of such particles should not last very long. However, *Pollack et al.* [1990] computed that the atmospheric CO_2 condensation rate could reach 5.10^{-5} kg m^{-2} s^{-}1 in a dusty atmosphere in the polar night. Despite the fact that most of this condensation is expected to occur at low altitudes, such a rate should be sufficient to maintain relatively large amount of CO_2 ice airborne. For instance, if we assume that the cloud particles are formed at only half the atmospheric scale height (3.5 km) and then fell, this rate would correspond to a rather thick cloud even for particles as big as 50 μm for which we then find $\tau_{20\mu\mathrm{m}} = 10$. In reality, the problem is more complex because CO_2 ice particles will continue to grow while falling down in a condensing atmosphere.

Precipitating clouds of pure CO_2 ice give more realistic spectra corresponding to T_{11} larger than T_{20} as observed in the IRTM data (Fig. 9). For particle radii larger than 20 μm, the scattering parameter Q_{scat} remains between 2 and 3.5 for wavenumbers greater than 200 cm^{-1}. Thus clouds composed of such particles exhibit a signature similar to the 25-μm curve on Fig. 8 characterized by a decrease of the brightness temperature with wavelength until the absorption bands near 100 cm^{-1}. This signature cannot match the observed

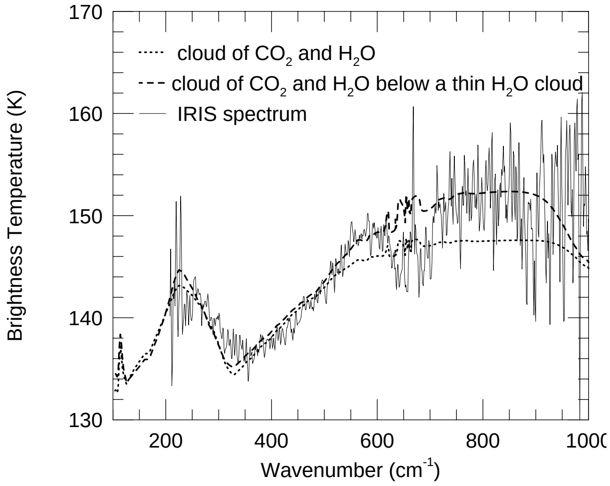

Figure 10. Same spectrum as in Fig. 1, compared to the simulated spectra of contaminated precipating CO_2 clouds. Dotted line shows the signature of a CO_2 ice cloud composed of 50-μm particles with a vertical optical thickness of 1.3 (0.06 kg.m^{-2}) mixed with 10 pr-μm of 1-μm water ice particles. The temperatures of cloud and ground are 148 K. Dashed line correspond to the same CO_2 ice cloud contaminated by only 5 pr-μm of 1-μm water ice particles lying below a thin water ice cloud of 0.5 pr-μm of 1-μm particles at 155 K.

IRIS spectra. However, we have found that small amounts of water ice (or dust) intimately mixed with the CO_2 ice particles would raise the emissivity of the cloud especially in their absorption bands. The presence of a water-ice absorption band centered at 220 cm^{-1} may therefore explain the shape of the IRIS spectra below 350 cm^{-1}. Fig. 10 shows the signature of such a precipitating cloud composed of CO_2 ice mixed with 10 precipitable microns (pr-μm) of water ice. Its signature is very similar to that of the IRIS spectrum. However, in the region from 600 to 1000 cm^{-1} , the contaminated CO_2 cloud model is flat or slightly decreasing while the IRIS spectrum shows an increase in brightness temperature peaking near 800 cm^{-1} at about 4 K above the 550-cm^{-1} temperature. Since the IRIS spectra all measure the North polar region in late winter, a thin water-ice polar hood cloud might be expected, based on historical observations. A cloud of 1-2-μm water-ice particles emits strongly at 800 cm^{-1}, much more weakly at 225 cm^{-1} (due to the Rayleigh limit), and is very transparent at other wavenumbers. A warmer water-ice cloud (consistent with the atmospheric temperature structure implied by the 15-μm gaseous CO_2 band) over the contaminated CO_2 snow raises the brightness temperature around 800-cm^{-1} and has little effect otherwise. The amount of cloud required is quite modest, less than one pr-μm or a visible optical depth below unity. For the IRIS spectrum shown in Fig. 10, the added cloud is at 155 K and has 0.5 pr-μm of 1-μm particles, and only 5 pr-μm are required to "contaminate" the CO_2 cloud and match the observed spectrum. We used optical constants for water ice at a temperature of 140 K [*Hudgins et al.*, 1993] rather than ones measured near 0^oC.

In Fig. 10, we have not tried to match the gaseous CO_2 band near 667 cm^{-1}. Fig. 11 gives us a closer look at this spectral region. In fact, the precipitating CO_2 clouds which appear to match the IRIS spectra are thought to have a temperature close to the ground temperature. Therefore they should lay at relatively low altitudes and their presence should not alter the atmospheric emission compare to that of an atmosphere free of CO_2 clouds. We have simulated the emission of the CO_2 atmosphere with a narrow-band model of the CO_2 15-μm band developed by *Hourdin* [1992] for Mars. The model is a classical random band model [*Goody*, 1964] with some improvements concerning the representation of Doppler effects. It is in very good agreement with a line-by-line model [*Hourdin*, 1992] and is very consistent with the results published by *Santee and Crisp* [1993] for the IRIS spectra.

A clear atmosphere scenario (and thus a low-altitude clouds scenario) can readily match the observed spectra. The dashed line on Fig. 11 was obtained with a simple atmospheric profile corresponding to a 6.6 mbar atmosphere following the CO_2 frost point temperature profile up to 0.4 mbar, and with a thermal inversion at 150-170 K above this level. Given the noise level in the IRIS data, the solution is far from being unique. Also, we found that the spectrum was not strongly affected by the thin, high-altitude water ice

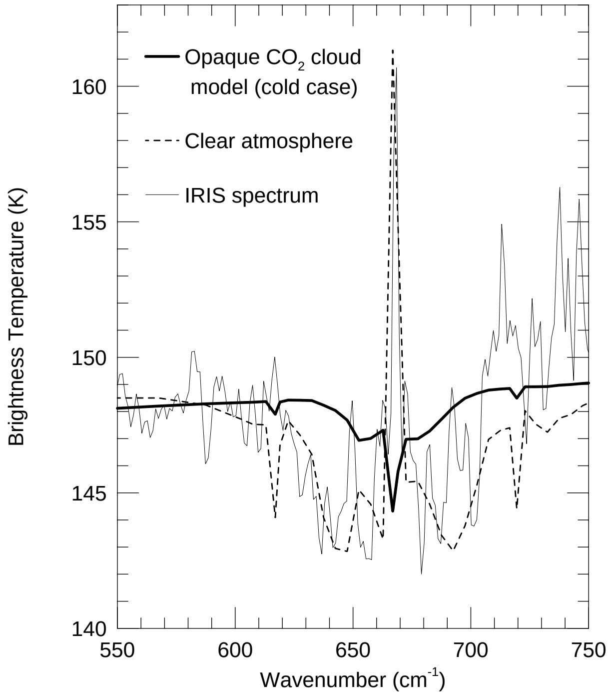

Figure 11. Comparison of the gaseous CO_2 band of the IRIS spectrum shown in Fig. 1 with model results. Dashed line is a best fit in a clear atmosphere case. Solid line is the atmospheric emission in the blackbody CO_2 cloud scenario. Despite the use of a temperature profile with minimum temperatures (the CO_2 frost point temperature profile), simulated brightness temperatures are too high in the band wings.

cloud suggested above to improve the match outside the 15-μm band.

4.6 Blackbody CO_2 Clouds

It has been suggested that CO_2 clouds could be optically very thick and efficient blackbody emitters like water clouds on Earth [*Paige et al.*, 1990]. Such a property would be puzzling. According to *Warren et al.* [1990], even for CO_2 ice deposits, large and even unrealistic amount of impurities would be required to reach a near unit emissivity. Nevertheless, we must admit that these criticisms are not conclusive. Viking observations showed that the CO_2 frost emissivity was near unity at least during late winter and spring [*Paige*, 1985]. The emissivity depends on many other aspects such as the grain shape. For instance, it seems reasonable that, if the growth can proceed in alternative ways, the form which maximizes the emissivity will be favored since such particles will cool, and grow at the maximum rate [*James et al.*, 1992].

To match the IRIS spectra within this context, *Paige et al.* [1990] proposed the following conceptual model based on an analysis of the IRIS spectra both inside and outside the CO_2 band. Near the ground and at low altitudes, the temperature profile stays close to the CO_2 frost point temperature and CO_2 clouds are present (Fig. 12). Above that, where the

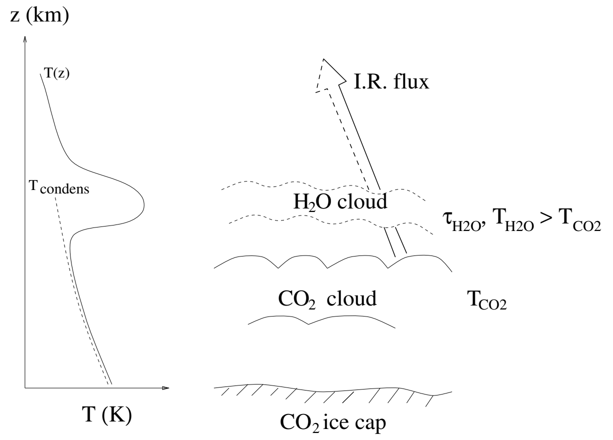

Figure 12. Schematic drawing of the opaque CO_2 cloud scenario and the corresponding model.

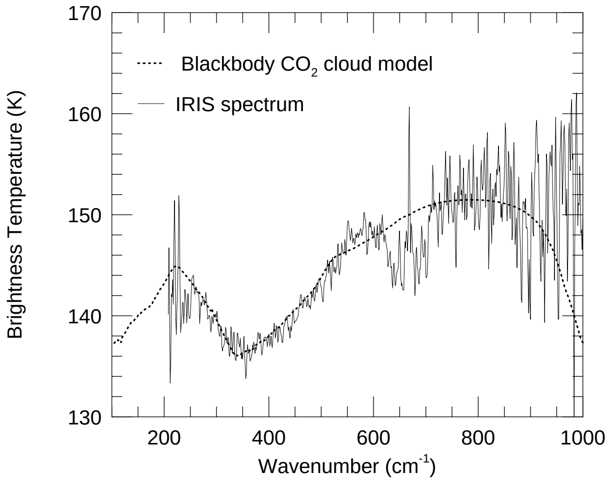

Figure 13. Same spectra than in Fig. 1, fitted by the blackbody CO_2 cloud model.

observed inversion occurs, the warmer upper atmosphere is relatively clear, but contains optically thin clouds of water ice. As the water ice cloud is warmer than the CO_2 clouds, it creates the feature seen in Fig. 1, the area around 350 cm^{-1} being a window between the two water ice absorption bands centered at 220 and 820 cm^{-1}. In this scenario, the anomalously cold brightness temperatures observed by Viking and Mariner 9 are explained directly by thermally opaque CO_2 clouds lying at one to several scale heights above the surface, at the CO_2 frost point temperature.

Comparison with the IRIS spectra outside the 15-μm band. To further study and verify the scenario suggested above, we have developed a simple model where the CO_2 / H_2O cloud system is defined by three parameters (Fig. 12) : T_{CO_2}, the temperature of the top of the blackbody CO_2 cloud, T_{H_2O}, the temperature of a warmer H_2O cloud lying above; τ_{H_2O}, the H_2O cloud vertical optical depth at 20 μm.

To compute how the CO_2 cloud emission is absorbed and scattered by the H_2O cloud, we have used the same radiative transfer program that we used for the previous CO_2 cloud calculations. Comparisons between an IRIS spectrum of the winter polar region and best fit simulations are shown in Fig. 13. The model can accurately reproduce the data. We needed to consider spherical water ice particles that were large enough (>2 μm) so that they scattered as well as absorbed and emitted thermal radiation. Here again, we used a Hansen-Hovenier gamma particle size distribution.

We have found CO_2 cloud temperatures ranging from 130 K to 140 K. T_{H_2O} and τ_{H_2O} are more difficult to infer separately because both tend to increase the H_2O cloud signature, although their effects are not identical. For example, the spectrum shown in Fig. 13 can be fitted with the couple (T_{H_2O}=160 K; τ_{H_2O}=0.4), or with (T_{H_2O}=180 K; τ_{H_2O}=0.1). Nevertheless, we can estimate that our modeled H_2O clouds have typical optical depths up to few tenths (1-2 pr-μm) and temperatures between 155 and 180 K. All these parameters seem realistic for northern winter.

Problem raised by the 15-μm gaseous CO_2 band. The blackbody CO_2 cloud / H_2O cloud simple model agree very well with the IRIS observations outside the 15-μm band. Is this scenario also consistent with the atmospheric emission in the 15-μm band? When the Martian atmosphere is clear, the high atmosphere produces most of the emitted radiance in the center of the band, and, in the more transparent band wings, the emitted radiation comes principally from the surface and near-surface layers. In the opaque CO_2 cloud scenario, things are quite different since the radiance is due to a combination of the emissions of the CO_2 cloud, the H_2O cloud and the atmospheric gaseous CO_2 atmosphere above the CO_2 cloud. The atmosphere and the ground below the CO_2 cloud level are hidden by the opaque CO_2 cloud.

We found that the atmosphere above the CO_2 cloud would not be able to create the cold brightness temperatures observed on each side of the core of the 15-μm band on most "cold" IRIS spectra. (143 K in Fig. 11, 5 K below the background continuum). This is illustrated by the thick line in Fig. 11, which shows the emission from an atmosphere following the coldest possible temperature profile (the CO_2 frost point temperature profile) above a CO_2 cloud at 135 K and below a theoretical H_2O cloud lying above the entire atmosphere. This temperature (135 K) is the highest temperature T_{CO_2} compatible with the IRIS spectrum used here. This should make it easier to match the cool wings, since the H_2O cloud properties are chosen in order to match the observed brightness temperature in the continuum outside the 15-μm band, i.e., below 600 cm^{-1}. Within this context, the warmer the CO_2 cloud is, the thinner and colder the H_2O cloud can be (and the thicker the atmosphere above the CO_2 cloud is). Despite the use of such parameters and despite the fact that we tend to underestimate the brightness temperatures by not taking the observed atmospheric inversion into account, the simulated spectrum (solid line) is well above the observed brightness temperatures.

In reality, things might be more complex than in the model, and, for example, the IRIS instrument could have observed more than just one CO_2 cloud / H_2O cloud system because of its large field of view. Nevertheless, no obvious reason can explain the cold brightness temperatures observed on the wings of the 15-μm band even if the IRIS instrument was observing a combination of various clouds and bare ground.

Comparison of the blackbody CO_2 cloud scenario with the IRTM data. T_{11} and T_{20} can be simulated from the spectra produced by the blackbody CO_2 cloud / H_2O cloud model. As the IRTM 20-μm band is near the minimum of absorption of water ice, in the 17-μm - 33-μm window, T_{20} is not strongly affected by the warmer H_2O clouds. Thus T_{20} measured by IRTM stays close to the effective CO_2 cloud temperature, although it is usually few Kelvins higher, especially for the coldest spots. On the other hand, the IRTM 11-μm band includes the strong water ice absorption band centered at 12.2-μm (820 cm^{-1}). T_{11} is much more affected by the water ice cloud than is T_{20}. On this basis, following our conclusion of section 2.2, the difference between T_{11} and T_{20} in this model is uniquely attributed to the presence of warmer H_2O clouds (at least, outside the dust storm periods).

Within this context the linear correlation between T_{20} and T_{11} shown in Fig. 6 would indicate that the $T_{11} - T_{20}$ signature of the water ice clouds is strongly correlated with the presence of CO_2 ice clouds (low T_{20}). The colder the CO_2 clouds are, the higher the temperature contrast between CO_2 and H_2O clouds is, and the stronger the H_2O cloud signature is. But this is not quantitatively sufficient. With a "constant" layer of H_2O clouds (constant temperature and opacity) lying above CO_2 clouds at various temperatures, our model cannot fully simulate the observed linear relation of $T_{11} - T_{20}$ to T_{20} (solid line with solid square symbols in Fig. 9). The properties of the H_2O clouds would have to be adjusted so that the signature of H_2O clouds disappears when CO_2 clouds are not present (T_{11} is close to T_{20} for higher values of T_{20}). This would suggest that the presence of CO_2 clouds is linked with the condensation of water ice, or with an increase of the temperature of the middle polar atmosphere inversion. No simple physical processes can be suggested to explain these observations. This raises another major problem for the CO_2 clouds hypothesis. More generally, it is difficult to understand why the IRTM instrument did not observe strong spectral contrast $T_{11} - T_{20}$ with a high value of T_{20}; in other words, why do thick H_2O clouds never occur above the ground without CO_2 clouds? Conversely the IRTM instrument did not measure T_{11} below 135 K, whereas T_{20} often reached temperatures below 130 or 125 K. This fact, which would mean that CO_2 clouds never occur without thick H_2O clouds above, would be also difficult to understand.

The blackbody CO_2 cloud hypothesis can also be compared with the IRTM observation in the 15-μm band. If the CO_2 cloud layer is an efficient blackbody emitter, T_{20} measured by IRTM should be close to the actual "thermodynamic" temperature of the observed CO_2 clouds, when CO_2 clouds are present. Therefore T_{20} should be approximately equal to the CO_2 frost point temperature of the top of the cloud, which depends on the pressure level of the cloud top. At 0.5 mbar, the CO_2 frost temperature is about 133 K. For a typical daytime temperature profile, and low emission angle, T_{15} also measures temperature at the 0.5 mbar level [*Kieffer et al.*, 1976a] Thus, when T_{20} is comparable to or below 133 K, we should have T_{15} close to T_{20}.

In Fig. 7a and 7b , we see indeed that when the IRTM is supposed to observe cold CO_2 clouds ($T_{20} < 135$ K), T_{15} remains between T_{20} and $T_{20} + 10$ K. As the temperature equivalent noise level for T_{15} is about 5 K at 133 K, we can consider that there is a good coincidence between T_{15} and T_{20}. These observations would support the blackbody CO_2 cloud scenario.

In Fig. 7c., which corresponds to the observations obtained during the polar warming event related to second Viking dust storm, there is no such correlation between T_{15} and T_{20}. Such observations, which could call into question the blackbody CO_2 cloud hypothesis since they suggest that very low brightness temperatures were observed where sufficiently cold CO_2 clouds could not exist, are puzzling, but not conclusive. Indeed, these unexpected values could be explained without contradicting this hypothesis. As explained by *Kieffer et al.* [1976a], T_{15} is supposed to sample the level about 0.6 mbar for vertical viewing for a typical daytime temperature profile. However, during a polar warming event, temperature profiles are far from typical. In our case, one can imagine a warm atmospheric layer above very cold CO_2 clouds at about 130 K. The thermal emission of the warm atmospheric layer would dominate the total emission of the atmosphere toward space in the 15-μm channel, even if the warm layer is above the 0.6 mbar-level. For instance, a system composed of an opaque CO_2 cloud at 130 K lying below a thermal inversion at 200 K would led to T_{15}=175 K. (Results obtained with the CO_2 gas narrow-band model of *Hourdin* [1992] presented in section 4.5 and an IRTM 15-μm band model, with an emission angle of 30^o, typical of the Viking Orbiter polar observations during the polar warming event.)

Conclusions for the blackbody CO_2 cloud scenario. Despite the fact that it can match the IRIS spectra oustside the 15-μm band, we have shown that the blackbody CO_2 cloud scenario is not consistent with some other key characteristics of the data in the 15-μm band and in the IRTM data. Besides, because modeling of the CO_2 clouds characteristics points strongly to semiopaque, scattering CO_2 clouds rather than absorbing clouds, and since these scattering clouds are more compatible with the observations, we believe that the blackbody CO_2 cloud hypothesis can be ruled out.

5. Low Surface Emissivity Hypothesis

5.1 CO_2 Frost Emissivity

Low emissivities are uncommon on known natural surfaces. As explained by *Warren et al.* [1990], most planetary surfaces have emissivities above 90% in the thermal infrared and in particular snow and sea-ice on Earth always have emissivities near 99%. Using spacecraft observations, *Paige* [1985] also estimated that the Martian polar cap emissivity was likely to be high. He studied the Viking IRTM data on restricted areas at both poles and found nearly coincident brightness temperatures at 11 μm and 20 μm during the early fall and late winter seasons. He showed that this could only be explained with a CO_2 ice emissivity close to one. In fact, this argument can be applied wherever T_{20} stayed close to T_{11}, which means outside the cold spots. Nevertheless Paige argued that the spatial and temporal variation of the low brightness temperatures would be very difficult to explain by spatial variations in surface emissivity.

However, CO_2 ice has the property that its interband absorption in the infrared is much smaller than, for example, that of H_2O ice, apparently because of the lack of hydrogen-bonding in CO_2 ice [*Warren*, 1986]. *Ditteon and Kieffer* [1979] measured that the transmissivity of CO_2 ice samples grown in the laboratory was quite high and estimated that the emissivity in the Viking IRTM 20-μm of pure CO_2 deposits was low enough to explain the cold spots. Since then, more sophisticated CO_2 snow models [*Warren et al.*, 1990] and more accurate laboratory measurements by G.B. Hansen (manuscript in preparation for *JGR-Planets*, 1995) have confirmed that Martian CO_2 frost could theoretically have an emissivity much lower than one in the thermal infrared.

The problem is complicated by other parameters. *Warren et al.* [1990] showed that water and dust contamination and large grain size could raise the modeled emissivity of CO_2 ice snow substantially, although they also showed that unrealistic amount of impurities (or large grain sizes to the order of one millimeter) would be required to get near unity. The emissivity may also depend on other properties, such as the the grain form, which is difficult to model. As explained for the CO_2 cloud particles, the form that maximizes the emissivity should be favored, since such deposits will cool, and grow at the maximum rate [*James et al.*, 1992].

5.2 Comparison With IRIS Spectra

Fig. 14 shows the spectral emissivity corresponding to the IRIS spectrum shown in Fig. 1, assuming that the thermodynamic temperature of the ground was the observed brightness temperature around 580-600 cm^{-1} (148 K in Fig. 1). The emissivity goes down to about 0.7 around 350-400 cm^{-1}. This value (0.7) is also typically observed on most other "cold" IRIS spectra.

In Fig. 14, the IRIS emissivity curve is compared to the emissivity of pure CO_2 ice deposits with various grain sizes. This is calculated using the same model as *Warren et al.* [1990] , but with the recent CO_2 ice optical constants of G. B. Hansen.

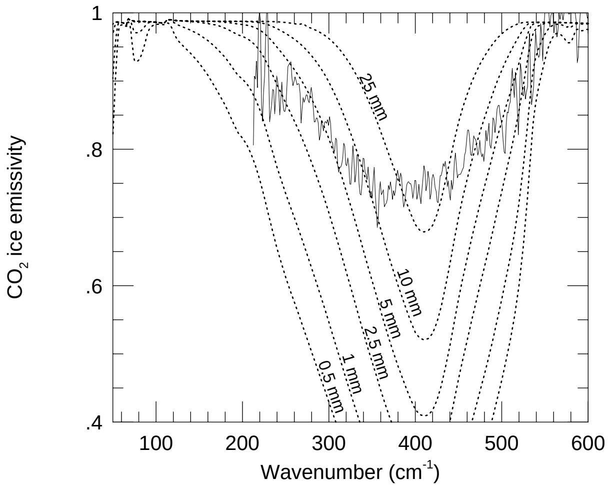

Figure 14. Spectral emissivity corresponding to the IRIS spectrum shown in Fig. 1 (solid line) compared to the spectral emissivity of CO_2 snow (dashed lines) calculated for various grain radii and a similar emission angle (60^0). The emissivity for the IRIS spectrum was estimated assuming that the thermodynamic temperature of the ground was 148K.

The model is of a semi-infinite layer of spherical particles using a delta-Eddington method [*Joseph et al.*, 1976]. No grain size of pure CO_2 will match the IRIS spectrum, but small amounts of water ice and dust particles intimately mixed with the CO_2 frost will have the effect of raising regions of low emissivity to higher levels, due to the infrared-opaque nature of these materials compared to CO_2 ice.

The approach is to start with the largest grain size possible so that only small amounts of dust and water need to be added to approximate the observed spectrum. The largest sizes are not appropriate, since their model emissivities are already higher than the IRIS spectrum at most wavenumbers. The pure CO_2 model spectra with grain radii from 1 to 2.5 mm are low enough at 250 and 500 cm^{-1} to be consistent with the IRIS spectrum. Adding about 0.1 % by weight of both water ice and dust (using the data for Montmorillonite 219b from *Toon et al.* [1977]). with effective grain radii of 10 and 2.5 μm, respectively, yields a model spectrum which approximates the IRIS data quite well (Fig. 15).

The model described above assumes that all particles are independent scatterers, and does not take close packing effects into account. This is mentioned by *Wiscombe and Warren* [1980], and a more rigorous treatment is presented by *Mishchenko* [1994], where it is shown that independent scattering calculations are valid for weakly absorbing particles much larger than the wavelength. Mishchenko also demonstrates that the scattering of packed nonspherical particles can be approximated by spheres of some equivalent size. If the scattering instead arises from imperfections and voids in

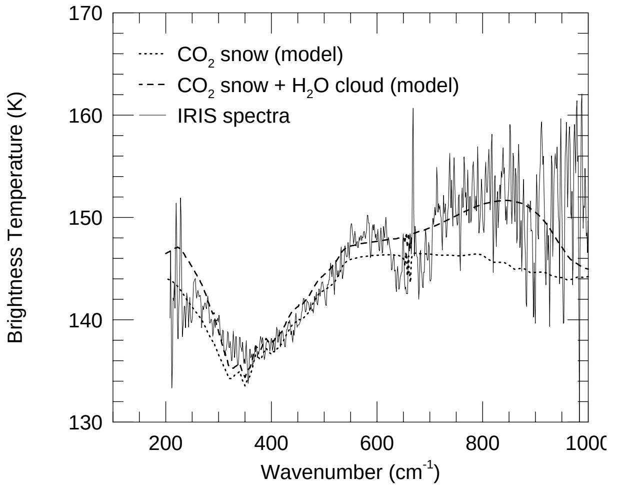

Figure 15. Same spectrum as in Fig. 1, compared to simulated spectra of contaminated CO_2 snow. Dotted line shows the signature of a mixture composed of CO_2 grains ($r = 2.5$-mm) mixed with 0.05 % of dust ($r = 2.5\mu$m) and 0.05 % of water ice ($r = 10\mu$m) at an emission angle of 60^o. Dashed line correspond to the same CO_2 ice snow lying below a thin cloud with 0.6 pr-μm of water ice particles ($r = 1\mu$m) at 155 K.

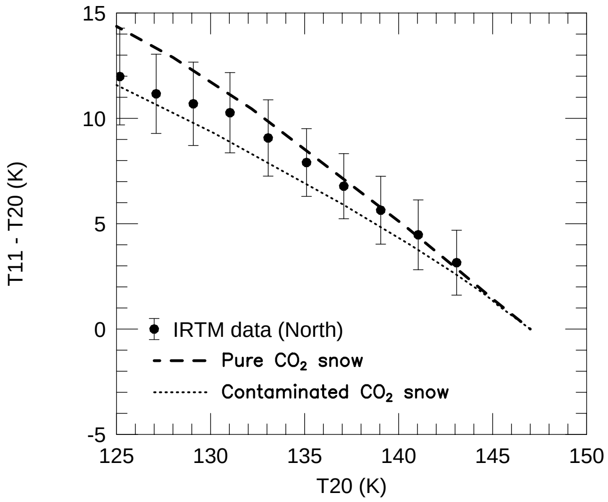

Figure 16. Correlation between T_{20} and T_{11} simulated with the pure and contaminated CO_2 frost model. Correlations were computed by varrying the grain size. The northern hemisphere IRTM data shown for comparison are the same as in Fig. 6.

a more monolithic deposit (perhaps more likely than large spherical particles when the inferred CO_2 grain size gets very large), the results may be different than those presented here. *Bohren* [1993] argues that transmission and reflection from bubbly water ice, at least, can be successfully modeled by independently scattering large spheres of some appropriate effective radius.

As for the contaminated precipitating CO_2 cloud, the contaminated CO_2 frost model also differs from the IRIS spectrum in the region from 600 to 1000-cm^{-1} (Fig. 15), where it is too flat. As in section 4.5, adding a thin warmer water ice cloud as expected in north polar region in late winter improves the fit.

Last, the low surface emissivity scenario corresponds to a clear atmosphere scenario and thus is consistent with the IRIS observations in the 15-μm band (Fig. 11)

5.3 Comparison With IRTM Data

As mentioned above the radiative properties of the ground should mainly be controlled by the frost grain size or shape. Fig. 16 illustrate the correlation of T_{11} and T_{20} simulated from both the pure and the contaminated CO_2 frost model for various grain sizes. The modeled correlation for pure CO_2 ice closely matches the observed systematic correlation between T_{11} and T_{20}. The contaminated CO_2 snow model has similar behavior to pure CO_2 when IRTM brightness temperatures are calculated, except that smaller CO_2 grain sizes can be used to achieve the same T_{11} and T_{20}. Centimeter-sized grains are still necessary to obtain near-blackbody values. The addition of thin water ice clouds mainly increases T_{11}, which shifts the model points upward on this graph.

6. Summary and Discussion: CO_2 Snow

In this paper, we have reviewed and modeled the possible scenarios related to the presence of CO_2 clouds or low surface emissivities. We have compared their spectral behavior to the observed spectral properties of the cold spots, characterized by the typical shape of the IRIS spectra and the systematic correlation between IRTM T_{11} and T_{20} (Table 2).

First, we have shown that nonprecipitating CO_2 clouds (whatever their ability to backscatter or absorb the infrared radiation) cannot match these observations. CO_2 clouds composed of small particles may exist but in most cases should be transparent because they cannot really scatter or absorb the infrared radiation outside the 15-μm band. The blackbody CO_2 cloud scenario proposed by *Paige et al.* [1990] (cold blackbody CO_2 clouds lying below thin warmer H_2O clouds) can match some of the observations, but several pieces of evidence presented in this paper allow us to rule out this scenario as well.

Nevertheless, we have found that precipitating CO_2 clouds with particle radii larger than 10 μm could produce the observed features, especially if they are contaminated by dust or water ice. Similarly, our simple modeling of the signature of CO_2 ice deposits in the infrared suggest that contaminated deposits could also match the observations. These two results are rather similar in that they both rely on the fact that large enough CO_2 ice grains can be efficient scatterers at infrared wavelengths, whether they are airborne or on the ground.

Aside from their spectral signatures, the cold spots are characterized by their high spatial and temporal variability,

	IRIS spectra shape outside the 15-μm band	IRIS spectra shape of the 15-μm band	IRTM data correlation between T_{11} and T_{20}
Small particle CO_2 clouds ($r < 10\mu$m)	no	yes	no
Precipitating CO_2 clouds ($r > 10\mu$m)	if contaminated by water	yes	yes (T_{20} varies with cloud thickness)
High altitude blackbody CO_2 cloud	yes (H_2O cloud above)	no (Cold wings)	requires correlation between CO_2 and H_2O clouds
Low emissivity CO_2 surface frost	if contaminated by water and dust	yes	yes (T_{20} varies with grain size)

Table 2. Ability of the various scenarios described in this paper to duplicate the spectral signatures of the cold spots.

and by their apparent link to atmospheric CO_2 condensation (correlation with the presence of dust and with the low atmospheric temperature T_{15} ; variability consistent with CO_2 atmospheric condensation modeling). Each of these points is consistent with the CO_2 clouds scenario and would tend to dismiss the low surface emissivity hypothesis.

However, we propose here a new realistic scenario consistent with both hypotheses. We have shown that the radiative properties of the CO_2 ice deposits are mainly controlled by the frost grain size or shape : the bigger the grains are, the higher the frost emissivity is. The CO_2 ice grain characteristics are likely to vary depending on wether the CO_2 ice condenses directly on the ground or in the atmosphere. On the ground, CO_2 condenses on CO_2 ice grains already existing and is likely to form dense, solid deposits composed of big CO_2 ice grains or even monolithic deposits. In the atmosphere, condensing CO_2 should form small particles which will fall down (See Table 1) while growing and continue to grow once on the ground, resulting in a layer of "fresh CO_2 snow." In fact, the average size of the CO_2 ice grain at the surface should mainly depend on the ratio between the atmospheric condensation rate and the total condensation rate. Since this fresh snow layer is expected to have low spectral emissivities compared to other areas where no atmospheric condensation (or no condensation at all) occurs, they are likely to create the observed cold brightness temperatures along with the CO_2 ice particles falling down from the atmosphere. Differentiating snow on the ground and snow in the atmosphere on the basis of spacecraft data may be very difficult. In particular, moderately low brightness temperatures can either be created by thinner precipitating CO_2 clouds or larger snow grains on the ground. When a snowfall ends, for instance, because the airborne dust has been washed out by the CO_2 ice precipitation (unlike on Earth where snowfall ends when there is no more water vapor in the atmosphere, there is always enough CO_2 in the Martian atmosphere), the CO_2 snow will age. The grain size will increase because of the continuing surface condensation which will tend to occur between the grains and aggregate them or because of a "destructive metamorphism" similar to what is observed for terrestrial water snow [*LaChapelle*, 1969] which do not require any condensation. More precisely, *Eluszkiewicz* [1993] showed that, because under martian conditions an inert gas is nearly absent and the frost temperature is nearly constant and thus no "air bubbles" and no thermal cracking are expected, the martian CO_2 snow seasonal metamorphism could form "nonporous, polycrystalline" layers, provided freshly condensed grains were sufficiently small. The spectral emissivities of the aging snow is thus likely to increase up to values close to unity until the next snowfall or until the spring. Within this context, the high variability of the cold spots cannot only be attributed to the variability of the atmospheric condensation but also to the ability of the CO_2 snow to age rapidly.

An interesting aspect of our study is the fact that the correlation between T_{20} and $T_{11} - T_{20}$ is rather similar for pure or contaminated CO_2 ice. This means that the cold spot signature seen by the IRTM instrument is independent of the CO_2 ice contamination by water or dust, unlike the shape of our simulated IRIS spectra. This could explain why the IRTM instrument always observed the same kind of correlation in both hemispheres and in all seasons in spite of the fact that the amount of airborne dust or water is highly variable. A spectrum obtained above the condensing south polar cap when less dust and water is expected than during the late northern winter observed by Mariner 9 may be very different than the IRIS data and closer to the pure CO_2 ice spectra shown in this paper.

Acknowledgments

We are very grateful to Terry Martin for providing the IRTM data and helping us to make the most of them. We wish to thank Bob Haberle, Frederic Hourdin, Hugh Kieffer, Jim Murphy, Dave Paige and Olivier Talagrand for helpful remarks and discussions as well as Maureen Bell, James Shaeffer, and Brad Sitton for their help. Special thanks to Michelle Santee, John Pearl and Shymala Dason who provided the IRIS data and Stephen Warren who reviewed the first draft. François Forget was supported by the French

Space Agency CNES during his sixteen month stay at the NASA Ames Research Center where a part of this work was done. This research was also supported in part by NASA's Planetary Atmospheres Program under grant RTOP 154-20-80-16.

References

Bohren, C. F., Colors of snow, frozen waterfalls, and icebergs, *J. Opt. Soc. Am.*, *73*, 1646–1652, 1983.

Briggs, G., K. Klaasen, T. Thorpe, and J. Wellman, Martian dynamical phenomenon during June-November 1976: Viking orbiter imaging results, *J. Geophys. Res.*, *82*, 4121–4149, 1977.

Briggs, G. A., and C. B. Leovy, Mariner 9 observations of the Mars north polar hood, *Bull. Am. Meteorol. Soc.*, *55*, 278–296, 1974.

Christensen, P. R., and R. W. Zurek, Martian north polar hazes and surface ice: Results from the Viking survey/completion mission, *J. Geophys. Res.*, *89*, 4587–4596, 1984.

Conrath, B., R. Curran, R. Hanel, V. Kunde, W. Maguire, J. Pearl, J. Pirraglia, J. Welker, and T. Burke, Atmospheric and surface properties of Mars obtained by infrared spectroscopy on Mariner 9, *J. Geophys. Res.*, *78*, 4267–4278, 1973.

Ditteon, R., and H. H. Kieffer, Optical properties of solid CO_2: Application to Mars, *J. Geophys. Res.*, *84*, 8294–8300, 1979.

Eluszkiewicz, J., On the microphysical state of the Martian seasonal caps, *Icarus*, *103*, 43–48, 1993.

Forget, F., and J. B. Pollack, Impact of the CO_2 and H_2O clouds of the Martian polar hood on the polar energy balance, in *Workshop on atmospheric transport on Mars (MSATT meeting)*, no. 93-05 in LPI Technical Report, pp. 16–17, Lunar and Planetary Institute, Houston, 1993.

Gierasch, P. J., and R. M. Goody, A study of the thermal and dynamical structure of the Martian lower atmosphere, *Planet. Space Sci.*, *16*, 615–646, 1968.

Goody, R. M., *Atmospheric Radiation, vol. I, Theoretical Basis*, Oxford University Press, New York, 1964.

Hanel, R., et al., Investigation of the Martian environment by infrared spectroscopy on Mariner 9, *Icarus*, *17*, 423–442, 1972.

Hansen, G. B., Low brightness temperatures of Martian polar deposits: New insight from recent measurement of CO_2 ice., *Bull. Am. Astron. Soc.*, *26*, 1114, 1994.

Hansen, J. E., and L. D. Travis, Light scaterring in planetary atmosphere, *Space Sci. Rev.*, *16*, 527–610, 1974.

Herr, K. C., and G. C. Pimentel, Evidence for solid carbon dioxide in the upper atmosphere of Mars, *Science*, *166*, 496–499, 1970.

Hess, S. L., Static stability and thermal wind in an atmosphere of variable composition: Application to Mars, *J. Geophys. Res.*, *84*, 2969–2973, 1979.

Hourdin, F., A new representation of the CO_2 15μm band for a Martian general circulation model, *J. Geophys. Res.*, *97*, 18,319–18,335, 1992.

Hudgins, D. M., S. A. Sanford, L. J. Allamandola, and A. G. G. M. Tielens, Mid and far-infrared spectroscopy of ices: Optical constants and integrated absorbances, *J. Astrophys. Jour. Suppl. Ser.*, *86*, 713–870, 1993.

Hunt, G. E., On the infrared radiative properties of CO2 ice clouds: Applications to Mars., *Geophys. Res. Lett.*, *7*, 481–484, 1980.

Jakosky, B. M., and T. Z. Martin, Mars: North-polar atmospheric warming during dust storms, *Icarus*, *72*, 528–534, 1987.

James, P. B., H. H. Kieffer, and D. A. Paige, The seasonal cycle of carbon dioxide on Mars, in *Mars*, pp. pp. 934–968, University of Arizona Press, Tucson, 1992.

Joseph, J. H., W. J. Wiscombe, and J. A. Weiman, The delta-eddington approximation for radiative flux transfer, *J. Atmos. Sci.*, *33*, 2452–2459, 1976.

Kieffer, H. H., S. C. Chase, E. D. Miner, F. D. Palluconi, G. Münch, G. Neugebauer, and T. Z. Martin, Infrared thermal mapping of the Martian surface and atmosphere: First results, *Science*, *193*, 780–786, 1976a.

Kieffer, H. H., P. R. Christensen, T. Z. Martin, E. D. Miner, and F. D. Palluconi, Infrared thermal mapping of the Martian surface and atmosphere: Viking observation of diurnal and geometric observation, *Science*, *194*, 1346–1351, 1976b.

Kieffer, H. H., T. Z. Martin, R. Peterfreund, B. M. Jakosky, E. D. Miner, and F. D. Palluconi, Thermal and albedo mapping during the Viking primary mission, *J. Geophys. Res.*, *82*, 4249–4291, 1977.

Kliore, A. J., D. L. Cain, G. Fjeldbo, B. L. Seidel, and M. J. Sykes, The atmosphere of Mars from Mariner 9 radio occultation measurements, *Icarus*, *17*, 484–516, 1972.

LaChapelle, E. R., *Field Guide to Snow Crystals*, University of Washington Press, Seattle, 1969., 1969.

Martin, T. Z., Mean thermal and albedo behavior of the Mars surface and atmosphere over a Martian year, *Icarus*, *45*, 427–446, 1981.

Martin, T. Z., and H. H. Kieffer, Thermal infrared properties of the Martian atmosphere, 2, the $15-\mu$m band measurements, *J. Geophys. Res.*, *84*, 2843–2852, 1979.

Mishchenko, M. I., Asymmetry parameters of the phase function for densely packed scattering grains, *J. Quant. Spectrosc. Radiat. Transfer*, *52*, 95–110, 1994.

Paige, D. A., *The annual heat balance of the Martian polar caps from Viking observations*, Ph.D. thesis, Calif. Inst. of Technol., Pasadena, 1985.

Paige, D. A., and A. P. Ingersoll, Annual heat balance of Martian polar caps: Viking observations, *Science*, *228*, 1160–1168, 1985.

Paige, D. A., D. Crisp, and M. L. Santee, It snows on Mars, *Bull. Am. Astron. Soc.*, *22*, 1075, 1990.

Pollack, J. B., R. M. Haberle, J. Schaeffer, and H. Lee, Simulations of the general circulation of the Martian atmosphere, 1, Polar processes, *J. Geophys. Res.*, *95*, 1447–1473, 1990.

Pollack, J. B., J. B. Dalton, D. Grinspoon, D. R. B. Wattson, R. Freedman, and D. Crisp, Near-infrared light from Venus nightside: A spectroscopic analysis, *Icarus*, *103*, 1–42, 1993.

Rossow, W. B., Cloud microphysics: Analysis of the clouds of Earth, Venus, Mars, and Jupiter, *Icarus*, *36*, 1,50, 1978.

Santee, M., and D. Crisp, Thermal structure and dust loading of the Martian atmosphere during late southern summer: Mariner 9 revisited, *J. Geophys. Res.*, *98*, 3261–3279, 1993.

Toon, O. B., J. B. Pollack, and C. Sagan, Physical properties of the particles composing the Martian dust storm of 1971-1972, *Icarus*, *30*, 663–696, 1977.

Toon, O. B., C. P. McKay, T. P. Ackerman, and K. Santhanam, Rapid calculation of radiative heating rates and photodissociation rates in inhomogeneous multiple scattering atmospheres, *J. Geophys. Res.*, *94*, 16,287–16,301, 1989.

Warren, S. G., Optical constants of carbon dioxide ice, *Appl. Opt.*, *25*, 2650–2674, 1986.

Warren, S. G., W. J. Wiscombe, and J. F. Firestone, Spectral albedo and emissivity of CO_2 in Martian polar caps: model results, *J. Geophys. Res.*, *95*, 717–741, 1990.

Wiscombe, W. J., and S. G. Warren, A model for the spectral albedo of snow, I, Pure snow, *J. Atmos. Sci.*, *37*, 2712–2733, 1980.

François Forget, Laboratoire de Météorologie Dynamique du CNRS, Université Paris 6, BP 99, 4 place Jussieu, 75252 Paris Cedex 05, France. (forget@lmd.jussieu.fr).

G. B. Hansen, Geophysics Program, University of Washington, Box 351650 Seattle, WA 98195-1650. (e-mail: ghansen@atmos.washington.edu).

March 13, 1995

This preprint was prepared with AGU's LaTeX macros v4, with the extension package 'AGU^{++}' by P. W. Daly, version 1.5g from 1998/09/14.